THE AMERICAN SOCIETY OF MECHANICAL ENGINEERS
345 E. 47 St., New York, N.Y. 10017

92-G

Calculation of Three-Dimensional Unsteady Flows in Turbomachinery Using the Linearized Harmonic Euler Equations

KENNETH C. HALL and CHRISTOPHER B. LORENCE

Department of Mechanical Engineering and Materials Science
Duke University
Durham, North Carolina 27706

ABSTRACT

An efficient three-dimensional Euler analysis of unsteady flows in turbomachinery is presented. The unsteady flow is modelled as the sum of a steady or mean flow field plus a harmonically varying small perturbation flow. The linearized Euler equations, which describe the small perturbation unsteady flow, are found to be linear, variable coefficient differential equations whose coefficients depend on the mean flow. A pseudo-time time-marching finite-volume Lax-Wendroff scheme is used to discretize and solve the linearized equations for the unknown perturbation flow quantities. Local time stepping and multiple-grid acceleration techniques are used to speed convergence. For unsteady flow problems involving blade motion, a harmonically deforming computational grid which conforms to the motion of the vibrating blades is used to eliminate large error-producing extrapolation terms that would otherwise appear in the airfoil surface boundary conditions and in the evaluation of the unsteady surface pressure. Results are presented for both linear and annular cascade geometries, and for the latter, both rotating and nonrotating blade rows.

NOMENCLATURE

AR	=	blade aspect ratio
$d\hat{\mathbf{A}}$	=	elemental area vector
$d\mathbf{A}$, $d\mathbf{A}'$	=	mean and perturbation elemental area vectors
D, ∂D	=	control volume and control surface
$d\hat{\mathcal{V}}$	=	elemental volume
$d\mathcal{V}$, $d\mathcal{V}'$	=	mean and perturbation elemental volume
$\hat{e}$	=	internal energy
f, g, h	=	grid motion perturbation functions
$\mathbf{f}$	=	$(f,g,h)^T$
$\hat{\mathbf{F}}$, $\hat{\mathbf{G}}$, $\hat{\mathbf{H}}$	=	flux vectors
$\mathbf{F}$, $\mathbf{G}$, $\mathbf{H}$	=	mean flow flux vectors
$\mathbf{F}'$, $\mathbf{G}'$, $\mathbf{H}'$	=	perturbation flow flux vectors
G	=	linear blade-to-blade gap
$\hat{I}$	=	rothalpy
M	=	Mach number
$\hat{\mathbf{n}}$	=	unit normal
$\overline{\mathbf{n}}$, $\mathbf{n}'$	=	mean and perturbation unit normals
$\hat{p}$	=	static pressure
P, p	=	mean flow and perturbation flow static pressures
r_H, r_T	=	hub and tip radii
$\hat{\mathbf{R}}$	=	surface displacement vector
$\hat{\mathbf{S}}$	=	source term vector
$\mathbf{S}$, $\mathbf{S}'$	=	mean flow and perturbation flow source terms
t	=	time
$\hat{u}$, $\hat{v}$, $\hat{w}$	=	Cartesian components of velocity
U, V, W	=	mean flow velocity components
u, v, w	=	perturbation flow velocity components
$\hat{\mathbf{U}}$	=	vector of conservation variables
$\mathbf{U}$, $\mathbf{u}$	=	mean and perturbation conservation variables
$\hat{\mathbf{V}}$	=	velocity vector
$\mathbf{V}$, $\mathbf{v}$	=	mean and perturbation velocity vectors
w_c	=	aerodynamic work per cycle per unit span
W_c	=	total aerodynamic work per cycle
x, y, z	=	Cartesian coordinates
x, θ, r	=	cylindrical coordinates
$\hat{\mathbf{x}}$	=	$(x,y,z)^T$
β	=	inflow angle relative to axial direction
γ	=	ratio of specific heats
Θ	=	stagger angle
Θ_G	=	angular blade-to-blade gap
ξ, η, ζ	=	computational coordinates
$\hat{\rho}$	=	static density
$\overline{\rho}$, ρ	=	mean flow and perturbation flow static densities
σ	=	interblade phase angle
τ	=	time in computational coordinates
ω, $\overline{\omega}$	=	dimensional and reduced frequencies
Ω	=	rotation rate of machine

Subscripts

a	=	axial direction
T	=	total or stagnation quantity
x, y, z	=	Cartesian directions
$\mathbf{x}$	=	due to grid motion
$\mathbf{u}$	=	due to perturbation in conservation variables
$-\infty$, ∞	=	far upstream and downstream regions

Presented at the International Gas Turbine and Aeroengine Congress and Exposition
Cologne, Germany June 1-4, 1992
This paper has been accepted for publication in the Transactions of the ASME
Discussion of it will be accepted at ASME Headquarters until September 30, 1992

INTRODUCTION

The ability to predict the aeroelastic phenomena of flutter and forced response is critical to the development of future generations of turbomachinery components including traditional fans, compressor and turbine stages, and unducted propfans. The aeromechanical behavior of these devices is strongly dependent on the unsteady aerodynamic behavior of the blade rows. Furthermore, the unsteady flow fields in these devices are inherently three-dimensional. New blade designs are becoming more three-dimensional with large amounts of twist and sweep. However, despite tremendous improvements in unsteady aerodynamic analyses over the past three decades, the accurate and efficient prediction of the unsteady aerodynamic behavior of realistic three-dimensional turbomachinery blade rows and propellers remains largely an unsolved problem.

Numerous two-dimensional analyses have been developed for flat-plate two-dimensional cascades operating in the incompressible (Whitehead, 1960 and 1962), subsonic (Smith, 1972; Whitehead, 1987), and supersonic (Verdon and McCune, 1975; Adamczyk and Goldstein, 1978) regimes. In these models, the steady flow field is assumed to be uniform. The equations that describe the small disturbance unsteady flow field are linear constant coefficient equations which can be solved analytically. These two-dimensional models are important since they are sometimes able to qualitatively predict certain types of flutter, notably unstalled supersonic torsional flutter in fans. However, because the models do not include the effects of steady blade loading, other forms of flutter, such as bending flutter, cannot be predicted.

Recently, three-dimensional semi-analytical methods have been developed to model unsteady flows in ducted fans (Namba, 1977; Chi, 1991). Like the classical two-dimensional flat plate methods, these models assume the airfoils carry no steady load. Namba and Toshimitsu (1987) included limited loading effects in their three-dimensional double linearization method. These analyses demonstrated that three-dimensional effects can significantly alter the behavior of the unsteady flow field.

Despite the limited success of the classical two- and three-dimensional models, they still do not provide a fully satisfactory solution to the aeromechanics problem. When the classical models are used, they must be used in conjunction with correlations based on experience to compensate for effects not included in the basic theories. This approach often works for relatively modest changes in blade design, but cannot be used with confidence for significantly new designs. Furthermore, the use of the two-dimensional methods in three dimensions usually requires the questionable assumption that they may be used in strip theory fashion.

Another approach which has been used to calculate unsteady periodic flows in cascades is to discretize the nonlinear fluid dynamic equations of motion on a computational grid which spans one or more blade passages. The discretized equations are then time-accurately time marched until all initial transients have decayed and a periodic state is reached. This approach has the advantage that many of the effects not included in the analytical models can be easily incorporated into the computational fluid dynamic (CFD) algorithm (e.g., arbitrary blade geometries, complicated shock structures, and various flow models). In recent years, a number of computational methods have been used to model unsteady flows in cascades. Several investigators have demonstrated the feasibility of time-accurately time marching the Euler equations (Fourmaux and Le Meur, 1987; Whitfield et al, 1987; Giles, 1988; Huff and Reddy, 1989) and Navier-Stokes equations (Huff, 1987; Rai, 1989a and 1989b) to analyze unsteady two- and three-dimensional flows in turbomachinery. However, due to the large number of grid points and the requirement than the analyses be both time-accurate and stable, these calculations are extremely expensive with supercomputer computational times measured in hours, days, or even weeks.

An alternative to the time-accurate time-marching methods, and the method used in this paper, is the linearized approach. In the linearized approach, the flow is assumed to be composed of a nonlinear mean or steady flow plus an unsteady perturbation flow. The linearized equations which describe the unsteady perturbation are linear variable coefficient equations for the unknown complex amplitude of the harmonic motion of the flow. A number of two-dimensional linearized harmonic potential (Whitehead and Grant, 1981; Verdon and Caspar, 1984; Hall and Verdon, 1991; Hall, 1992) and linearized harmonic Euler codes (Ni and Sisto, 1976; Hall and Crawley, 1989; Hall and Clark, 1991a and 1991b; Holmes and Chuang, 1991) have been developed to analyze the flutter and forced response of turbomachinery blade rows. Work on two-dimensional linearized harmonic Euler solvers has demonstrated the large computational time savings that can be achieved using linearized techniques while still modelling the dominant physics. For example, for a typical gust response problem, the linearized Euler technique is nearly two orders of magnitude faster than a time-marching Euler code and gives very similar predictions of the unsteady flow (Hall and Crawley, 1989).

While providing some qualitative and quantitative insight into the mechanisms of flutter and forced response, all of the linearized potential and Euler solvers developed to date have been two-dimensional. In this paper, we present a fully three-dimensional linearized Euler analysis capable of predicting unsteady flows in turbomachinery due to vibratory blade motion and incoming gusts (only the blade motion problem is considered here). The three-dimensional linearized Euler equations are derived for the general case of a rotating frame of reference. To solve the linearized Euler equations, we use the pseudo-time time-marching technique suggested by Ni and Sisto (1976). One advantage of this approach is that the equations become hyperbolic in pseudo time so that existing time-marching algorithms can be employed to efficiently solve the linearized Euler equations. In this paper, the linearized equations are solved very efficiently using using a Lax-Wendroff scheme with local time stepping and multiple-grid acceleration (Ni and Bogoian, 1989).

Another important feature of the present analysis is the use of a deforming computational grid. Although deforming computational grids have been used in nonlinear time-marching analyses (Huff, 1987; Huff and Reddy, 1989; Batina, 1990), until recently, most linearized analyses have used computational grids fixed in space. For fixed-grid analyses of flutter problems, an additional term must be added to the airfoil boundary conditions to extrapolate the flow variables from the boundary of the grid to the instantaneous location of the airfoil. This extrapolation term contains the gradient of the mean flow velocity which is difficult to compute accurately, especially around the leading and trailing edges of the blade. One way to eliminate the extrapolation terms is to use a grid which continuously deforms with the airfoil. Whitehead and Grant (1981) used a transformed perturbation potential in their linearized harmonic potential analysis. The transformation can be viewed as equivalent to using a computational grid which undergoes rigid body motion which conforms to the motion of plunging and pitching airfoils. Recently, Hall (1992) developed a potential solver based on a linearized variational principle that includes the effects of a deformable computational grid which conforms to both rigid body and flexible blade motions. Hall and Clark (1991a, 1991b) and Holmes and Chuang (1991) have recently applied the deforming grid technique to the two- dimensional linearized Euler

technique. In this paper, we extend the deforming grid technique to three dimensions.

Results are presented in this paper that demonstrate the accuracy and efficiency of the method, and demonstrate the effects of three-dimensionality on unsteady flows in turbomachinery. Results are presented for both stationary and rotating cascades. Preliminary results indicate that three-dimensional effects are very important, and that strip theory may, in some cases, seriously overpredict the aerodynamic damping of vibrating blades.

THEORETICAL APPROACH

Flow Field Description

For many flows of interest in turbomachinery aeroelasticity, viscous effects are confined to thin boundary layers near the blade and casing surfaces. Under these circumstances, the Euler equations – which represent the conservation of mass, momentum, and energy for an inviscid, adiabatic flow – are a useful model of the flow field. Consider a Cartesian coordinate system with its x axis aligned with the axis of rotation of a blade row. The y and z axes rotate about the x axis with speed Ω, the rotational speed of the blade row. The nonlinear Euler equations in the rotating frame of reference are given by

$$\frac{\partial \hat{\mathbf{U}}}{\partial t} + \frac{\partial \hat{\mathbf{F}}}{\partial x} + \frac{\partial \hat{\mathbf{G}}}{\partial y} + \frac{\partial \hat{\mathbf{H}}}{\partial z} - \hat{\mathbf{S}} = 0 \tag{1}$$

where $\hat{\mathbf{U}}$ is the vector of conservation variables, $\hat{\mathbf{F}}$, $\hat{\mathbf{G}}$, and $\hat{\mathbf{H}}$ are the so-called flux vectors, and $\hat{\mathbf{S}}$ is a vector of source terms. These vector quantities are given by

$$\hat{\mathbf{U}} = \begin{bmatrix} \hat{\rho} \\ \hat{\rho}\hat{u} \\ \hat{\rho}\hat{v} \\ \hat{\rho}\hat{w} \\ \hat{e} \end{bmatrix}, \quad \hat{\mathbf{F}} = \begin{bmatrix} \hat{\rho}\hat{u} \\ \hat{\rho}\hat{u}^2 + \hat{p} \\ \hat{\rho}\hat{u}\hat{v} \\ \hat{\rho}\hat{u}\hat{w} \\ \hat{\rho}\hat{u}\hat{I} \end{bmatrix}, \quad \hat{\mathbf{G}} = \begin{bmatrix} \hat{\rho}\hat{v} \\ \hat{\rho}\hat{u}\hat{v} \\ \hat{\rho}\hat{v}^2 + \hat{p} \\ \hat{\rho}\hat{v}\hat{w} \\ \hat{\rho}\hat{v}\hat{I} \end{bmatrix},$$

$$\hat{\mathbf{H}} = \begin{bmatrix} \hat{\rho}\hat{w} \\ \hat{\rho}\hat{u}\hat{w} \\ \hat{\rho}\hat{v}\hat{w} \\ \hat{\rho}\hat{w}^2 + \hat{p} \\ \hat{\rho}\hat{w}\hat{I} \end{bmatrix}, \quad \hat{\mathbf{S}} = \begin{bmatrix} 0 \\ 0 \\ \hat{\rho}\left(\Omega^2 y + 2\Omega\hat{w}\right) \\ \hat{\rho}\left(\Omega^2 z - 2\Omega\hat{v}\right) \\ 0 \end{bmatrix}$$

where $\hat{\rho}$ is the density, $\hat{p}$ is the pressure, $\hat{u}$, $\hat{v}$, and $\hat{w}$ are the x, y, and z components of velocity, $\hat{e}$ is the internal energy, and $\hat{I}$ is the rothalpy. The source terms that appear in the y and z momentum equations represent centrifugal and Coriolis forces. In this form, the effects of rotation appear explicitly in only the source terms. However, the pressure, $\hat{p}$, and the rothalpy, $\hat{I}$, are also functions of the rotation rate, i.e.,

$$\hat{p} = (\gamma - 1)\left[\hat{e} - \frac{1}{2}\hat{\rho}\left(\hat{u}^2 + \hat{v}^2 + \hat{w}^2\right) + \frac{1}{2}\hat{\rho}\Omega^2 r^2\right] \tag{2}$$

and

$$\hat{I} = \frac{\hat{e} + \hat{p}}{\hat{\rho}} = \frac{\gamma}{\gamma - 1}\frac{\hat{p}}{\hat{\rho}} + \frac{1}{2}\left(\hat{u}^2 + \hat{v}^2 + \hat{w}^2\right) - \frac{1}{2}\Omega^2 r^2 \tag{3}$$

Here r is the distance from the x axis ($r = \sqrt{y^2 + z^2}$). Note that the flux vectors and source terms depend not only on the conservation variables and the rotation rate, but also on the *position* of the fluid particle, that is, $\hat{\mathbf{F}} = \hat{\mathbf{F}}(\hat{\mathbf{U}}, \hat{\mathbf{x}})$ where $\hat{\mathbf{x}} = (x, y, z)^T$.

For finite-volume calculations, the integral form of the Euler equations is more convenient. Integrating the nonlinear Euler equations [Eq. (1)] over a deforming control volume, D, bounded by the control surface, ∂D, gives after some manipulation

$$\frac{\partial}{\partial t}\iiint_D \hat{\mathbf{U}}\, d\hat{\mathcal{V}} + \iint_{\partial D}\left[\left(\hat{\mathbf{F}} - \hat{\mathbf{U}}\frac{\partial f}{\partial t}\right) d\hat{A}_x + \left(\hat{\mathbf{G}} - \hat{\mathbf{U}}\frac{\partial g}{\partial t}\right) d\hat{A}_y + \left(\hat{\mathbf{H}} - \hat{\mathbf{U}}\frac{\partial h}{\partial t}\right) d\hat{A}_z\right] - \iiint_D \hat{\mathbf{S}}\, d\hat{\mathcal{V}} = 0 \tag{4}$$

Here f, g, and h are the x, y, and z displacements in the position of the control surface; and $d\hat{A}_x$, $d\hat{A}_y$, and $d\hat{A}_z$ are the scalar components of the elemental surface vector $d\hat{\mathbf{A}}$; and $d\hat{\mathcal{V}}$ is the elemental volume of the control volume.

The conventional method used to solve the unsteady nonlinear Euler equations for the case of a temporally periodic disturbance is to discretize the equations using finite-volume operators, and to time-accurately time march the discretized equations until any initial solution transients have disappeared leaving behind the desired periodic solution. Because of the requirement that the unsteady solution be both time-accurate and stable, however, the computational time required to solve the three-dimensional Euler equations using this approach is prohibitively large for design applications.

Fortunately, for many unsteady flows of interest in turbomachinery aeroelasticity applications, the unsteadiness in the flow is small compared to the mean flow and the source of the unsteadiness is harmonic or periodic. Hence, we will shortly make the assumption that the conservation variables may be represented as the sum of a mean flow plus a harmonic small perturbation unsteady flow.

In the present analysis, the computational grid conforms to the motion of the airfoils (for the flutter problem). Hence, the grid is assumed to undergo small harmonic deformation about its steady position, i.e.,

$$x(\xi, \eta, \zeta, \tau) = \xi + f(\xi, \eta, \zeta)e^{j\omega\tau} \tag{5}$$

$$y(\xi, \eta, \zeta, \tau) = \eta + g(\xi, \eta, \zeta)e^{j\omega\tau} \tag{6}$$

$$z(\xi, \eta, \zeta, \tau) = \zeta + h(\xi, \eta, \zeta)e^{j\omega\tau} \tag{7}$$

$$t(\xi, \eta, \zeta, \tau) = \tau \tag{8}$$

where f, g, and h are the first-order amplitudes of grid motion about the mean positions, ξ, η, and ζ.

Having defined the motion of the computational coordinate system, the unsteady flow field is now represented by the first-order perturbation series

$$\hat{\mathbf{U}}(\xi, \eta, \zeta, \tau) = \mathbf{U}(\xi, \eta, \zeta) + \mathbf{u}(\xi, \eta, \zeta)e^{j\omega\tau} \tag{9}$$

where $\mathbf{U}$ is the vector of mean or steady flow conservation variables, $\mathbf{u}$ is the vector of first-order perturbations in the conservation variables, and ω is the frequency of excitation. The mean flow and perturbation flow variables may be thought of as "attached" to the harmonically deforming computational grid. Therefore, an observer in the fixed coordinate system (x, y, z) sees unsteadiness in the flow due to both the unsteady perturbation in the conservation variables, $\mathbf{u}$, and the deformation of the mean flow field, $\mathbf{U}$.

Substitution of the perturbation assumptions [Eqs. (5)-(9)] into the expression for the flux vector $\hat{\mathbf{F}}$ results in the first-order perturbation series

$$\hat{\mathbf{F}} = \mathbf{F} + \left(\mathbf{F}'_{\mathbf{u}} + \mathbf{F}'_{\mathbf{x}}\right) e^{j\omega\tau} \tag{10}$$

where $\mathbf{F}$ is the mean flow flux vector, $\mathbf{F}'_{\mathbf{u}}$ is the first-order perturbation in the flux vector due to the first-order perturbation in the conservation variables, $\mathbf{u}$, and $\mathbf{F}'_{\mathbf{x}}$ is the perturbation in the flux vector due to the grid motion, $\mathbf{f}$. These perturbation fluxes are given by

$$\mathbf{F}'_{\mathbf{u}} = \frac{\partial \mathbf{F}}{\partial \mathbf{U}}\mathbf{u} \tag{11}$$

and

$$\mathbf{F}'_{\mathbf{x}} = \frac{\partial \mathbf{F}}{\partial \mathbf{x}}\mathbf{f} \tag{12}$$

where

$$\frac{\partial \mathbf{F}}{\partial \mathbf{U}} = \begin{bmatrix} 0 & 1 & 0 & 0 & 0 \\ -U^2 + \frac{\gamma-1}{2}V_T^2 & -(\gamma-3)U & (1-\gamma)V & (1-\gamma)W & \gamma-1 \\ -UV & V & U & 0 & 0 \\ -UW & W & 0 & U & 0 \\ -U(I - \frac{\gamma-1}{2}V_T^2) & I-(\gamma-1)U^2 & (1-\gamma)UV & (1-\gamma)UW & \gamma U \end{bmatrix}$$

and

$$\frac{\partial \mathbf{F}}{\partial \mathbf{x}} = \begin{bmatrix} 0 & 0 & 0 \\ 0 & (\gamma-1)\overline{\rho}\Omega^2\eta & (\gamma-1)\overline{\rho}\Omega^2\zeta \\ 0 & 0 & 0 \\ 0 & 0 & 0 \\ 0 & (\gamma-1)\overline{\rho}U\Omega^2\eta & (\gamma-1)\overline{\rho}U\Omega^2\zeta \end{bmatrix}$$

Here U, V, and W are the mean flow velocity components, V_T is the mean flow velocity magnitude, and I and $\overline{\rho}$ are the mean flow rothalpy and density, respectively. Note that the perturbation flux term $\mathbf{F}'_{\mathbf{x}}$ is zero for the case of a non-rotating frame of reference since the entries in the $\partial\mathbf{F}/\partial\mathbf{x}$ matrix are proportional to the rotation rate squared. Similar perturbation series exist for the remaining flux vectors, $\hat{\mathbf{G}}$ and $\hat{\mathbf{H}}$, and the vector of source terms, $\hat{\mathbf{S}}$.

Substitution of the perturbation series for the conservation variables, grid motion, flux vectors and source terms into the integral form of the nonlinear Euler equations and collection of zeroth- and first-order terms gives the mean flow and linearized unsteady Euler equations, respectively. The mean flow Euler equations are given by

$$\iint_{\partial D} (\mathbf{F}, \mathbf{G}, \mathbf{H}) \cdot d\mathbf{A} - \iiint_D \mathbf{S}\, d\mathcal{V} = 0 \tag{13}$$

where $d\mathbf{A}$ and $d\mathcal{V}$ are the elemental area vector and elemental volume of the undeformed (mean) control volume. Similarly, the integral form of the linearized Euler equations is

$$j\omega \iiint_D \mathbf{u}\, d\mathcal{V} + \iint_{\partial D} \left(\frac{\partial \mathbf{F}}{\partial \mathbf{U}}\mathbf{u}, \frac{\partial \mathbf{G}}{\partial \mathbf{U}}\mathbf{u}, \frac{\partial \mathbf{H}}{\partial \mathbf{U}}\mathbf{u}\right) \cdot d\mathbf{A} - \iiint_D \frac{\partial \mathbf{S}}{\partial \mathbf{U}}\mathbf{u}\, d\mathcal{V} =$$

$$-j\omega \iiint_D \mathbf{U}\, d\mathcal{V}' - \iint_{\partial D} (\mathbf{F}, \mathbf{G}, \mathbf{H}) \cdot d\mathbf{A}' - \iint_{\partial D} (\mathbf{F}'_{\mathbf{x}}, \mathbf{G}'_{\mathbf{x}}, \mathbf{H}'_{\mathbf{x}}) \cdot d\mathbf{A}$$

$$+ j\omega \iint_{\partial D} \mathbf{U}\mathbf{f} \cdot d\mathbf{A} + \iiint_D \mathbf{S}\, d\mathcal{V}' + \iiint_D \mathbf{S}'_{\mathbf{x}}\, d\mathcal{V} \tag{14}$$

where $d\mathbf{A}'$ and $d\mathcal{V}'$ are the first-order perturbations in the elemental area vector and elemental volume of the deforming control volume. Here we have grouped homogeneous terms in the unknown perturbation $\mathbf{u}$ on the left-hand side and inhomogeneous terms on the right-hand side. The terms on the right-hand side of Eq. (14) arise from the motion of the grid and are identically zero for the case of a fixed grid. Note that the linearized harmonic Euler equations are time invariant; time does not appear explicitly since the equations have been cast in the frequency domain.

Near-Field Boundary Conditions

Having developed the governing equations of the unsteady perturbation flow, we next consider the near-field boundary conditions. Because the linearized Euler equations are linear, modes of blade motion or gusts may be superposed. Hence, without loss of generality, we assume the unsteady flow to have a fixed interblade phase angle, σ, from blade to blade. The flow field may then be solved in a single blade passage by applying complex periodicity conditions along the upstream and downstream periodic boundaries. For linear cascades which extend in the y direction, the complex periodicity condition takes the form

$$\mathbf{u}(x, y+G, z) = \mathbf{u}(x, y, z)e^{j\sigma} \tag{15}$$

where G is the blade-to-blade gap. For annular cascades, the periodicity condition is expressed as

$$\mathbf{u}(x, \theta+\Theta_G, r) = \mathbf{T}\mathbf{u}(x, \theta, r)e^{j\sigma} \tag{16}$$

where Θ_G is the angular distance between adjacent blades, and $\mathbf{T}$ is a matrix which rotates the velocity vector in the y, z plane through the angle Θ_G.

On the airfoil surfaces, we must ensure that no mass flows through the surface. The nonlinear solid wall boundary condition is given by

$$\hat{\mathbf{V}} \cdot \hat{\mathbf{n}} - \frac{\partial \hat{\mathbf{R}}}{\partial t} \cdot \hat{\mathbf{n}} = 0 \tag{17}$$

where $\hat{\mathbf{R}}$ is the position vector that desribes the position of the airfoil surface, and $\hat{\mathbf{n}}$ is the surface unit normal. Expanding Eq. (17) in a perturbation series and collecting terms of first-order gives the linearized flow tangency condition

$$\mathbf{v} \cdot \overline{\mathbf{n}} = -\mathbf{V} \cdot \mathbf{n}' + j\omega\mathbf{r} \cdot \overline{\mathbf{n}} \tag{18}$$

where $\mathbf{V}$ and $\mathbf{v}$ are the mean flow and perturbation flow velocities, respectively, $\overline{\mathbf{n}}$ and $\mathbf{n}'$ are the mean and perturbation unit normals, and $\mathbf{r}$ is the perturbation in the position of the airfoil surface. Since the grid motion conforms to the motion of the airfoil, the perturbation in the blade position may be expressed as $\mathbf{r} = \mathbf{f}$. The first term on the right-hand side of Eq. (18) is the upwash due to blade rotation. The second term is the upwash due to the translational velocity of the blade. Note that because a deforming grid is used, the usual velocity extrapolation term found in fixed grid analyses does not appear. Also, Eq. (18) applies to all solid surfaces, not just airfoils. Hence, if the grid motion is such that the grid slides across curved surfaces, such as the hub or tip casing, then there will be an upwash required on these surfaces as well, even though the casing surfaces do not vibrate.

NUMERICAL SOLUTION METHOD

The general solution procedure is as follows. First, a three-dimensional H-grid is generated in a single blade passage of the cascade. The mean flow field is computed using a conventional steady Euler solver. Then, for each interblade phase angle, vibratory mode shape, and reduced frequency of interest, the grid motion is prescribed. The mean flow field and prescribed grid motion are then used to form the variable coefficients and the inhomogeneous part of the linearized Euler equations. Finally, the linearized Euler equations are discretized and solved on the steady computational grid.

Grid Generation

The computational grids used in this investigation are body-fitted H-grids. Although C and O-type grids are commonly used in steady flow calculations, these grids lack the resolution in the far-field to adequately resolve acoustic, vortical, and entropic waves. H-grids, on the other hand, provide good resolution throughout the computational domain.

The mean flow (steady) computational grid is generated using a combination of algebraic and elliptic grid generation techniques. The grid points on the airfoil surfaces are generated algebraically. The grid points on the upstream and downstream periodic boundaries and on the far-field boundaries are generated using transfinite interpolation. Finally, the grid points on the hub and tip casings and in the interior are generated using an elliptic grid generation technique based on the work of Thompson et al (1974).

For unsteady flow problems involving blade motion, the grid motion $\mathbf{f}$ must also be specified, subject to a number of constraints. The motion of the grid must conform to the motion of the airfoils, and the motion of the grid at the periodic boundaries must satisfy complex periodicity. The grid may slide along the casing surfaces, but must have no component of motion normal to the casing. Finally, to simplify the application of the far-field boundary conditions, the motion of the grid in the far-field of the computational domain should go to zero. In the interior, the motion of the grid may be somewhat arbitrary, although for computational accuracy, a smooth distribution of grid motion is preferred. For this reason, Laplace's equation is used to describe the motion of the interior of the grid, i.e.,

$$\nabla^2 \mathbf{f} = 0 \tag{19}$$

A finite element scheme is used to discretize Laplace's equation on the steady computational grid, and the resulting system of linear equations is solved using successive line over-relaxation (SLOR). Note that since the grid motion is harmonic, the motion need only be calculated once prior to the solution of the linearized Euler equations.

Pseudo-Time Time Marching

Having defined the computational grid, solved for the mean flow field, and computed the unsteady grid motion, we next consider the integration of the linearized Euler equations. Note that because the linearized Euler equations [Eq. (14)] are solved in the frequency domain for a single frequency, ω, time derivatives are replaced by the operator $j\omega$. Furthermore, the unsteady perturbation $\mathbf{u}$ is time invariant. Hall and Crawley (1989) discretized the two-dimensional linearized Euler equations using a finite volume operator and solved the resulting large sparse linear system very efficiently using Gaussian elimination. In three dimensions, this approach would lead to a system of equations with an extremely large bandwidth, and hence, would be too expensive to solve using a direct method. Instead, we solve the three-dimensional linearized Euler equations using the pseudo-time technique originally proposed by Ni and Sisto (1976). Using this method, the perturbation conservation variables, $\mathbf{u}$, are assumed to be functions of both space and time so that Eq. (9) becomes

$$\hat{\mathbf{U}}(\xi,\eta,\zeta,\tau) = \mathbf{U}(\xi,\eta,\zeta) + \mathbf{u}(\xi,\eta,\zeta,\tau)e^{j\omega\tau} \tag{20}$$

Substitution of Eq. (20) into the nonlinear Euler equations and collection of first-order perturbation terms leads to the pseudo time dependent linearized Euler equations

$$\frac{\partial}{\partial\tau}\iiint_D \mathbf{u}\,d\mathcal{V} + j\omega\iiint_D \mathbf{u}\,d\mathcal{V} + \iint_{\partial D}\left(\frac{\partial \mathbf{F}}{\partial \mathbf{U}}\mathbf{u}, \frac{\partial \mathbf{G}}{\partial \mathbf{U}}\mathbf{u}, \frac{\partial \mathbf{H}}{\partial \mathbf{U}}\mathbf{u}\right)\cdot d\mathbf{A} - \iiint_D \frac{\partial \mathbf{S}}{\partial \mathbf{U}}\mathbf{u}\,d\xi\,d\eta\,d\zeta = \mathbf{b} \tag{21}$$

where $\mathbf{b}$ is the right-hand side of Eq. (14). Note that Eq. (21) is now hyperbolic in time. Furthermore, as time advances, $\mathbf{u}$ reaches a steady-state value so that the first term of Eq. (21) goes to zero and the solution to Eq. (14) is recovered. The advantage of this approach is that any of a number of well developed time marching algorithms can be used to solve the linearized Euler equations. Furthermore, since only the steady-state solution is desired, local time stepping and multiple-grid acceleration techniques can be used to speed convergence. The result is that the linearized Euler equations can be solved in a fraction of the time required to solve the unsteady flow problem by time-accurately time marching the nonlinear Euler equations.

We use a three-dimensional Lax-Wendroff scheme (Ni and Bogoian, 1989) to discretize and solve both the steady Euler and linearized unsteady Euler equations. The scheme is a second-order accurate, node-centered scheme that uses both local time stepping and multiple-grid acceleration. A combination of second and fourth difference smoothing is used to eliminate sawtooth modes and capture shocks. (For the subsonic cases reported in this paper, only fourth difference smoothing was used.)

Nonreflecting Far-Field Boundary Conditions

In the present unsteady linearized analysis, we assume that the blade row is isolated in an infinitely long annular duct. The computational domain is, by necessity, finite in extent. At the far-field computational boundaries, nonreflecting boundary conditions are required to prevent spurious reflections of outgoing pressure, entropy, and vorticity waves back into the computational domain. For two-dimensional problems, the behavior of the linearized equations can be be described analytically (e.g., Verdon et al, 1975; Hall and Crawley, 1989; Giles, 1990) and then matched to the numerical solution at the far-field. For three-dimensional flow fields, however, the wave propagation behavior is known analytically for only a few special cases; no general analytical expression has been derived for the three-dimensional problem.

In this investigation, we follow the approach of Saxer and Giles (1990) and apply approximate nonreflecting boundary conditions at the far-field. We in effect unroll each radial station on the far-field computational boundary and treat it as if it were two-dimensional. Furthermore, the source terms arising from rotation are neglected. We then apply the "exact" nonreflecting boundary conditions originally developed for two-dimensional linearized Euler solvers. After each iteration, the solution at each radial station is transformed into a sum of Fourier modes. (Fourier modes are the eigenmodes of two-dimensional wave propagation.) Each Fourier mode is further decomposed into characteristics representing two acoustic waves, two vorticity waves, and an entropy wave. At this point, those characteristics which correspond to waves entering from outside of the computational domain are set to zero. The remaining modes are then inverse Fourier transformed to obtain the desired solution at the far-field boundary. In two-dimensions, this process produces exact nonreflecting boundary conditions to within truncation error. In three-dimensions, however, some reflections will occur, especially if there are significant radial variations in the solution.

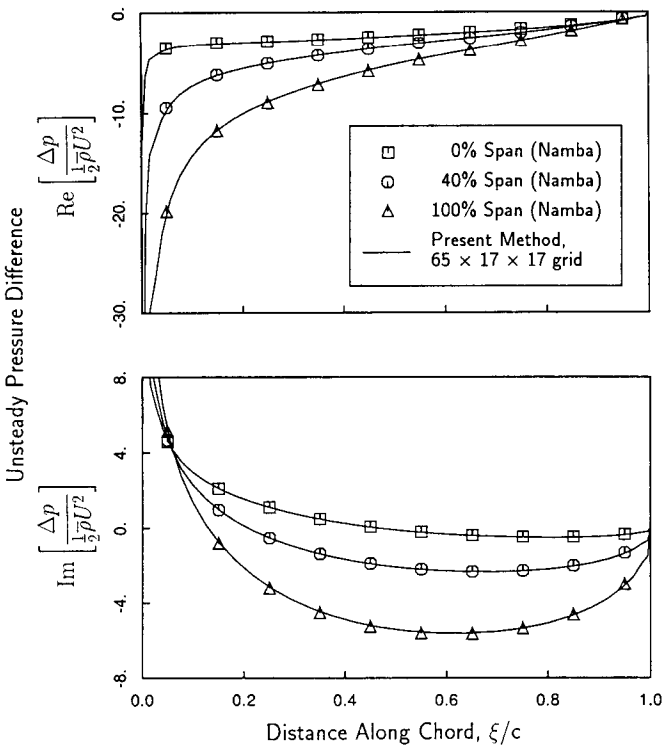

Figure 1: Unsteady pressure distribution on surface of reference airfoil of linear flat-plate cascade with airfoils pitching about leading edge. Pitching distribution is linear from hub to tip. $\Theta = 45°$, $AR = 3.0$, $M = 0.7$, $\overline{\omega} = 1.0$, $\sigma = 180°$.

RESULTS

In this section, a number of test cases are presented to examine the accuracy of the linearized Euler analysis and to demonstrate the effects of three-dimensionality on unsteady flows. Unsteady flows due to blade motion (the aerodynamic damping problem) in both linear and annular cascade geometries are presented. The aerodynamic damping is important for both the flutter and forced response problems. Unless otherwise indicated, the results were computed on 65 × 17 × 17 node computational grids using three levels of multiple-grid acceleration.

Linear Flat-Plate Cascade

To test the accuracy of the present method, we first consider the case of a linear cascade of flat-plate airfoils vibrating in torsion. The stagger angle of the airfoils, Θ, is 45°, the aspect ratio, AR, is 3.0 and the gap-to-chord ratio, G, is 1.0. The airfoils are aligned with the mean flow. Hence, the mean flow through the cascade is uniform. For the case considered here, the mean flow Mach number, M, is 0.7. The airfoils vibrate in torsion about their leading edge with a reduced frequency, $\overline{\omega}$, of 1.0, based on chord and upstream velocity, and an interblade phase angle, σ, of 180°. The distribution of pitching amplitude is linear from hub to tip. Figure 1 shows the computed unsteady pressure difference across the airfoil surface. Also shown are the results of the semi-analytical three-dimensional method developed by Namba (1987). Note the extremely good agreement between the linearized Euler results and Namba's method, even near the leading edge where there is a square root singularity in the solution. These results demonstrate

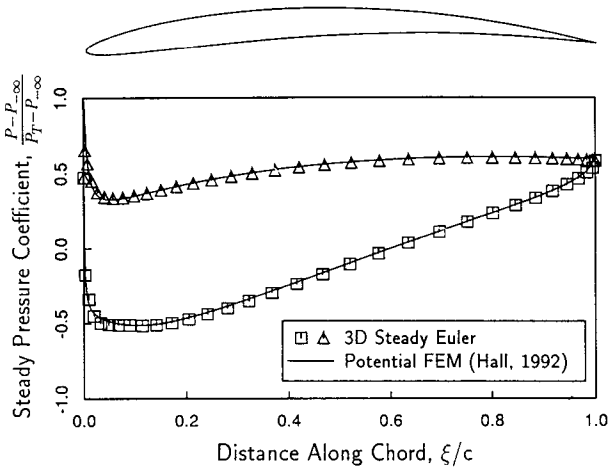

Figure 2: Mean pressure distribution on surface of airfoils of Standard Configuration No. 10 cascade. $G = 1.0$, $\Theta = 45°$, $AR = 2.0$, $\beta_{-\infty} = 55°$, $M_{-\infty} = 0.7$.

the ability of the linearized Euler analysis to model accurately unsteady flows due to three-dimensional vibratory mode shapes, at least for the case of lightly loaded cascades.

Subsonic Linear Compressor

To verify that the present three-dimensional linearized Euler analysis works properly in the limit of two-dimensional cascades with steady loading, we consider a linear cascade of compressor blades. The cascade considered here is the newly designated Standard Configuration No. 10, one in a series of standard turbomachinery aeroelastic test cases for validating unsteady aerodynamic theories (Bölcs and Fransson, 1986; Fransson, 1991). The airfoils of this cascade have a circular arc camber distribution with a maximum height of 5 percent of the chord. The thickness distribution is that of a NACA 0006 airfoil slightly modified so that the trailing edge is wedged. The gap-to-chord ratio, G, is 1.0, and the stagger, Θ, is 45°. For the present three-dimensional analysis, we selected an aspect ratio, AR, of 2.0. The steady inflow Mach number, $M_{-\infty}$, is 0.7, and the inflow angle, $\beta_{-\infty}$, measured from the axial direction is 55°. Figure 2 shows the computed steady pressure on the blade surface. Also shown for comparison is the pressure computed using a two-dimensional full potential method (Hall, 1992) on a 129 × 33 node computational grid. The two solutions are seen to agree very well. The maximum Mach number on the suction surface of the airfoil is about 0.92.

Having computed the mean flow solution, we now consider the case of the cascade of airfoils vibrating in plunge normal to the chord line with a reduced frequency, $\overline{\omega}$, of 1.0, and an interblade phase angle, σ, of 180°. For the first case considered, the motion is two-dimensional, that is, the motion is uniform from hub to tip. Shown in Fig. 3 are the real and imaginary parts of the computed unsteady pressure distribution on the surface of the reference airfoil. Also shown is the unsteady pressure distribution computed using the two-dimensional linearized potential method due to Hall (1992). Note the good agreement between the two theories indicating that the present analysis produces the proper results, at least in the limit of two-dimensional flow. Also note that the solution is well behaved in the vicinity of the leading and trailing edges despite the use of a fairly coarse grid. This well-behaved solution results from using a deforming computational

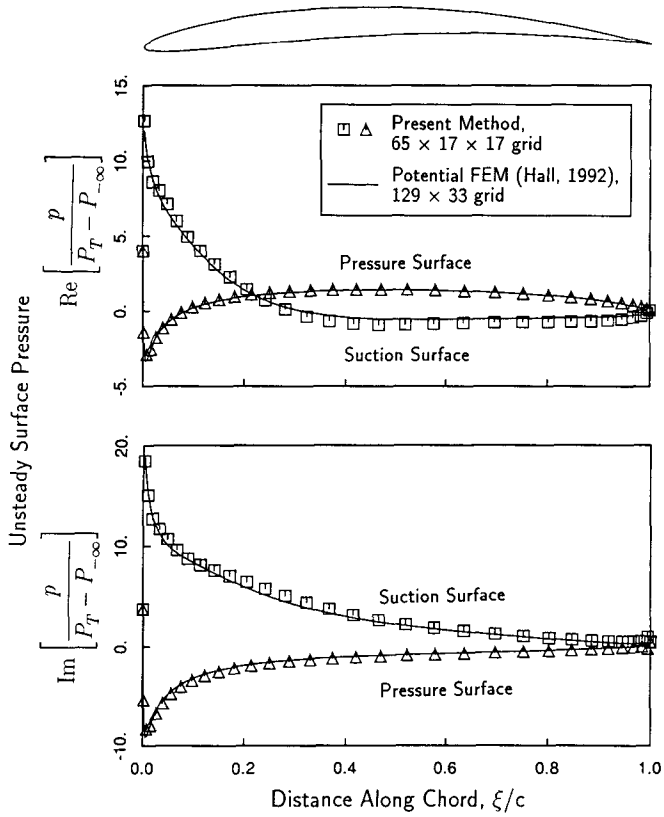

Figure 3: Unsteady pressure distribution on reference airfoil of Standard Configuration No. 10 cascade with airfoils undergoing plunging motion. Plunging motion is uniform from hub to tip. $\overline{\omega} = 1.0$, $\sigma = 180°$.

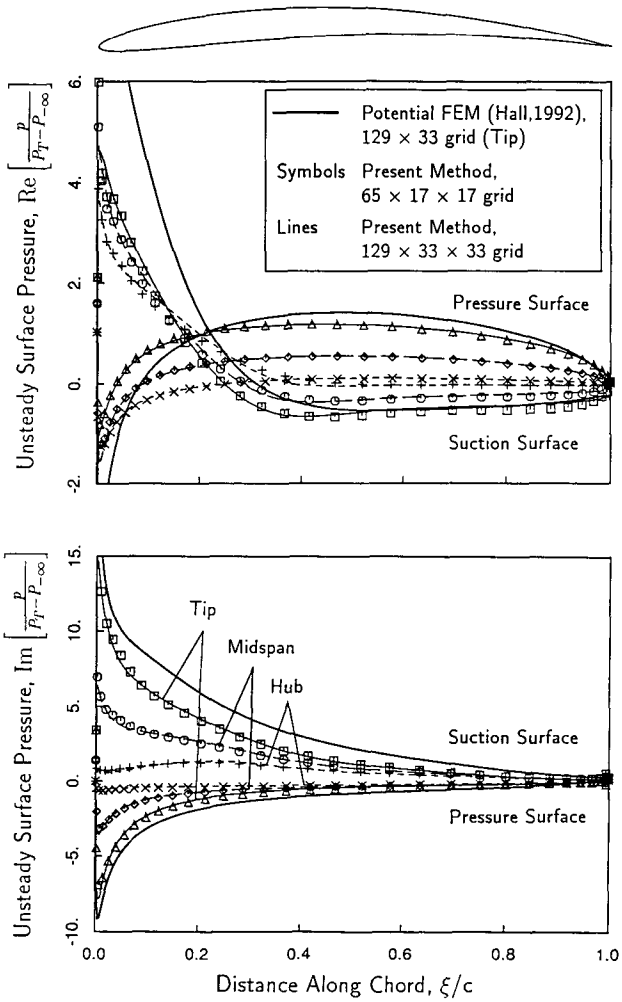

Figure 4: Unsteady pressure distribution on surface of reference airfoil of Standard Configuration No. 10 cascade with airfoils vibrating in first bending mode. $\overline{\omega} = 1.0$, $\sigma = 180°$.

grid. Such high quality solutions would be difficult to obtain on a coarse fixed grid.

Next, we consider the same linear compressor cascade, but now prescribe the blade motion to be three-dimensional. The blades vibrate with the first-bending mode shape of a cantilevered beam. The mode shape is normalized such that the displacement at the tip is unity. Again, the reduced frequency, $\overline{\omega}$, is 1.0 and the interblade phase angle, σ, is 180°. Shown in Fig. 4 are the real and imaginary parts of the unsteady pressure distribution at three spanwise stations. These results were computed using two different computational grids of differing resolution to assess the accuracy of the solution. The solution computed on the $65 \times 17 \times 17$ node grid is seen to be nearly identical to that computed on the $129 \times 33 \times 33$ node grid. For low reduced frequencies, the accuracy of the solution is dominated by the accuracy of the solution around the leading and trailing edges. On a length scale comparable to the radius of the leading edge, the flow around the leading edge appears quasi-steady. Hence, if a deforming grid is used, the accuracy of the unsteady solution will be on a par with the accuracy of the steady flow solution, at least for low to moderate reduced frequencies. If a fixed grid were used, extrapolation terms in the airfoil boundary conditions would reduce the accuracy of the solution. At higher reduced frequencies, the resolution of the grid must be sufficient throughout the computational domain to resolve short wavelength disturbances.

Also shown for comparison in Fig. 4 is the unsteady pressure distribution computed using Hall's two-dimensional linearized potential analysis at the tip section. Note that the response at the blade tip is larger than the response at the hub as would be expected from a strip theory analysis. However, the spanwise gradient in the pressure distribution is somewhat smaller than would be predicted by strip theory. Namba (1987) shows that this reduction in the spanwise gradient is due to the trailing streamwise vorticity. Also, comparing these results to Hall's, the shape of the imaginary part of the pressure distribution – that is, the part in phase with the upwash – is fairly well predicted by strip theory. The shape of the real part of the pressure distribution – the part out of phase with the upwash – is somewhat different than that predicted by strip theory.

Figure 5 shows convergence histories for the previous case computed on the $65 \times 17 \times 17$ node computational grid. Without multiple-grid acceleration, but with local time stepping, the steady and unsteady solutions converge at approximately the same rate. With multiple-grid acceleration, both the steady and unsteady convergence rates are dramatically improved, although the unsteady solution converges at about half the rate of the steady solution. Although it is not yet clear why this difference occurs, the computational savings are still quite substantial. Using three levels of multiple-grid acceleration, the steady solution required

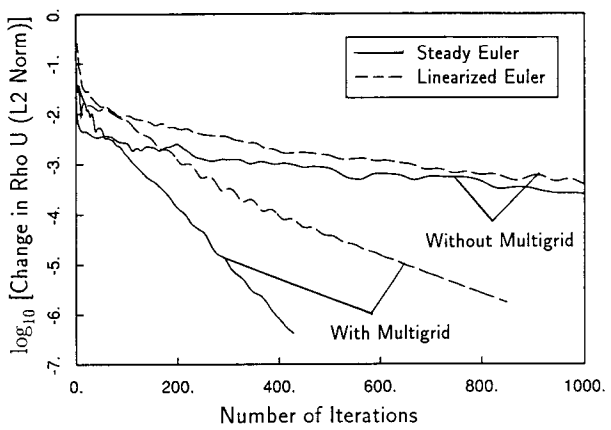

Figure 5: Convergence histories for steady and unsteady solutions shown in Figs. 2 and 4.

about 44 minutes of CPU time to converge on a Stardent 3000 workstation while the unsteady solution required about 294 minutes. It should be pointed out that these codes are not vectorized nor optimized. Nevertheless, these computer times are considerably shorter than would be required to time-accurately time march the nonlinear Euler equations. The large computational savings stem from the fact that only the steady state solution to the linearized harmonic Euler equations is desired, and hence, both local time stepping and multiple-grid acceleration techniques may be used.

Low Speed Linear Compressor

The next cascade considered is a linear cascade of Joukowski-like airfoils (Gostelow, 1984) operating in the low subsonic regime. The gap-to-chord ratio, G, is 0.990, the stagger angle, Θ, is 37.5°, and the aspect ratio, *AR*, is 2. For this example, the inflow angle, $\beta_{-\infty}$, is 53.5°, and the inflow Mach number, $M_{-\infty}$, is 0.25. The airfoils vibrate in pitch about their midchords with a linear distribution in amplitude from hub to tip. The reduced frequency, $\overline{\omega}$, is 0.4 and the interblade phase angle, σ, is 180°. Figure 6 shows the computed unsteady pressure distribution at three radial stations on the airfoil. Also shown for comparison is the unsteady pressure distribution computed using Hall's two-dimensional linearized potential analysis at the tip section. The shape of the real part of the unsteady pressure distribution agrees quite well with the strip theory results. The magnitude of the response increases from hub to tip as one would expect, although the pressure is nonzero at the hub and the magnitude at the tip is somewhat smaller than predicted by strip theory. The imaginary pressure distribution, on the other hand, is not well predicted by strip theory. The amplitudes of the response are approximately equal at the three radial stations. Furthermore, the shape of the distribution is somewhat different from the strip theory results.

Figure 7 shows the unsteady aerodynamic work done per cycle on the airfoil for a range of interblade phase angles (negative work per cycle corresponds to positive aerodynamic damping). The shape is nearly sinusoidal indicating that the airfoil is primarily influenced by its own motion and that of its two neighbors. Figure 7 also shows the work per cycle obtained using a linearized potential method applied in strip theory fashion. Note that the strip theory solution has a shape similar to the linearized Euler results, but the magnitude of the work is significantly overpredicted, especially for large negative interblade phase angles typical of those encountered in forced response problems.

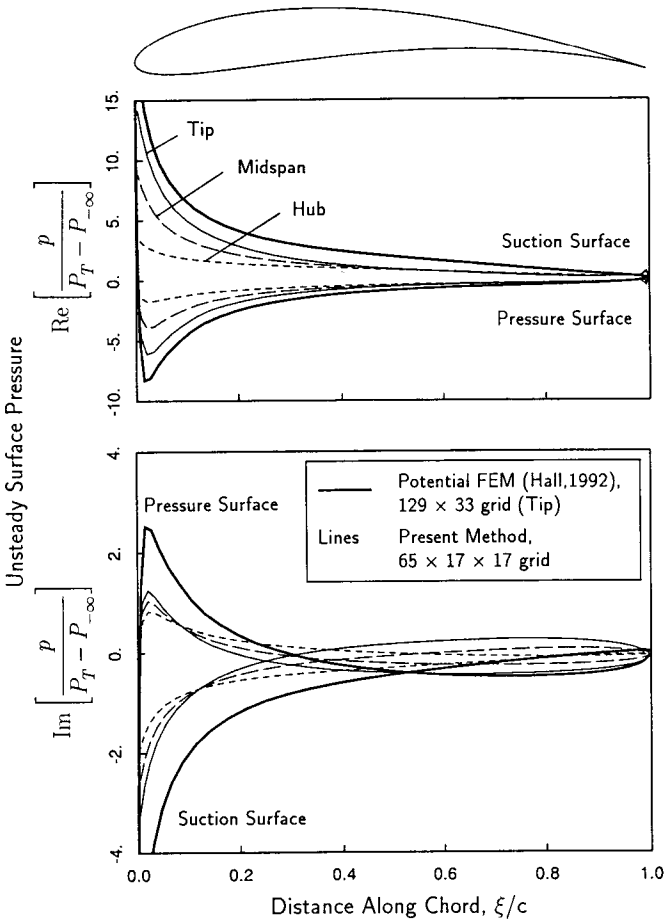

Figure 6: Unsteady pressure distribution on surface of reference airfoil of Gostelow cascade with airfoils pitching about midchord. Pitching distribution is linear from hub to tip. $\overline{\omega} = 0.4$, $\sigma = 180°$.

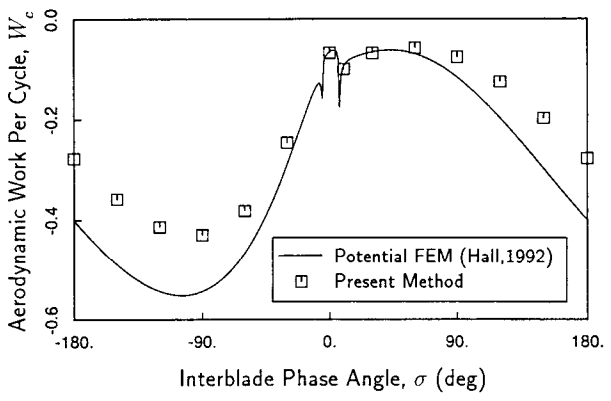

Figure 7: Total aerodynamic work per cycle on reference airfoil of Gostelow cascade with airfoils pitching about midchord. Pitching distribution is linear from hub to tip. $\overline{\omega} = 0.4$.

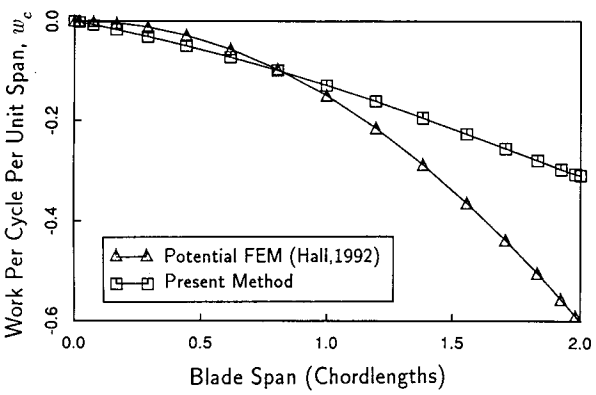

Figure 8: Aerodynamic work per cycle per unit span on reference airfoil of Gostelow cascade with airfoils pitching about midchord. Pitching distribution is linear from hub to tip. $\overline{\omega} = 0.4$, $\sigma = 180°$.

Figure 8 shows the distribution of aerodynamic work along the span of the blade for the case where the airfoils vibrate in pitch with a reduced frequency, $\overline{\omega}$, of 0.4 and an interblade phase angle, σ, of $-180°$. Note that strip theory significantly overpredicts the work done near the tip of the airfoil. This is not surprising since the imaginary part of the pressure distribution at the tip of the airfoil is overpredicted by strip theory.

High Speed Experimental Turbine

In this section, we compare our computational results to the experimental data for the Fourth Standard Configuration, a high speed turbine studied by Bölcs and Fransson (1986). Although the geometry is that of a turbine, the annular blade row did not rotate in their experiment. Instead, inlet guide vanes induced swirl in the flow to produce the proper inflow angle. The stagger angle, Θ, is 56.6°, the hub to tip ratio, r_H/r_T, is 0.8, the number of blades, N, is 20, and the aspect ratio, AR, is 0.538. The blades have a uniform shape from hub to tip. Bölcs and Fransson measured both mean and unsteady surface pressures while the turbine blades vibrated in a plunging motion with a fixed interblade phase angle. For the case considered here (Fourth Standard Configuration, Case 2), the reported inflow angle, $\beta_{-\infty}$, at the midspan is 45° and the inflow mach number, $M_{-\infty}$, is 0.26. The exit flow angle, β_{∞}, is 72° and the exit Mach number, M_{∞}, is 0.76. A number of investigators have found that the mean flow computational results match the experimental mean pressure distribution better if the inflow angle is taken to be 50°, and we will use this inflow angle as well.

Figure 9 shows the computed mean flow solution at three radial stations along the blade. Also shown is the experimental data taken at the midspan station. The computational results of the present steady Euler solver are seen to be in good agreement with the experimental data. Also note the variation in loading from hub to tip. The swirl induced in the flow by the inlet guide vanes and subsequent turning of the inlet duct from the radial to axial direction produces a free vortex flow. Hence, the inflow angle is greater at the hub than at the tip.

Having calculated the steady flow, we computed the unsteady flow due to a plunging motion of the airfoils in a direction nearly perpendicular to the chord line with an interblade phase angle, σ, of 90° and a reduced frequency, $\overline{\omega}$, of 0.13 based on chord and nominal exit velocity. The blade in the experimental setup is hinged well below the hub. Hence, the motion at the hub is nonzero. We took the displacement to be unity at the midspan, 0.703 at the hub, and 1.307 at the tip. Shown in Fig. 10 are the magnitude

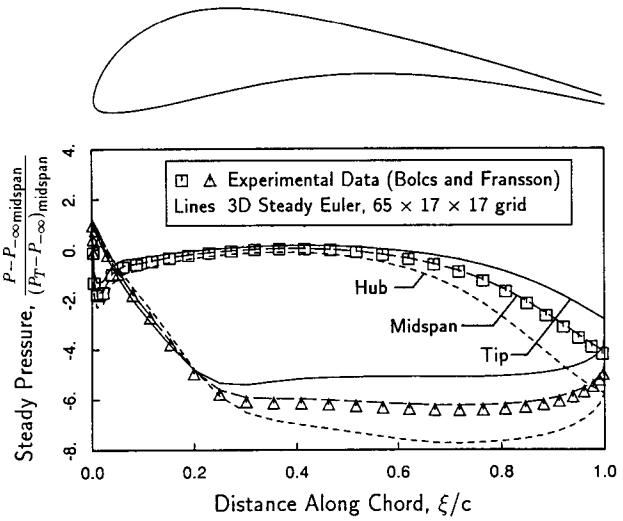

Figure 9: Mean pressure distribution on surface of airfoils of Fourth Standard Configuration turbine cascade. $N = 20$, $r_H/r_T = 0.8$, $\Theta = 56.6°$, AR= 0.538, $\beta_{-\infty} = 50°$, $M_{-\infty} = 0.26$, $\beta_{\infty} = 72°$, $M_{\infty} = 0.76$.

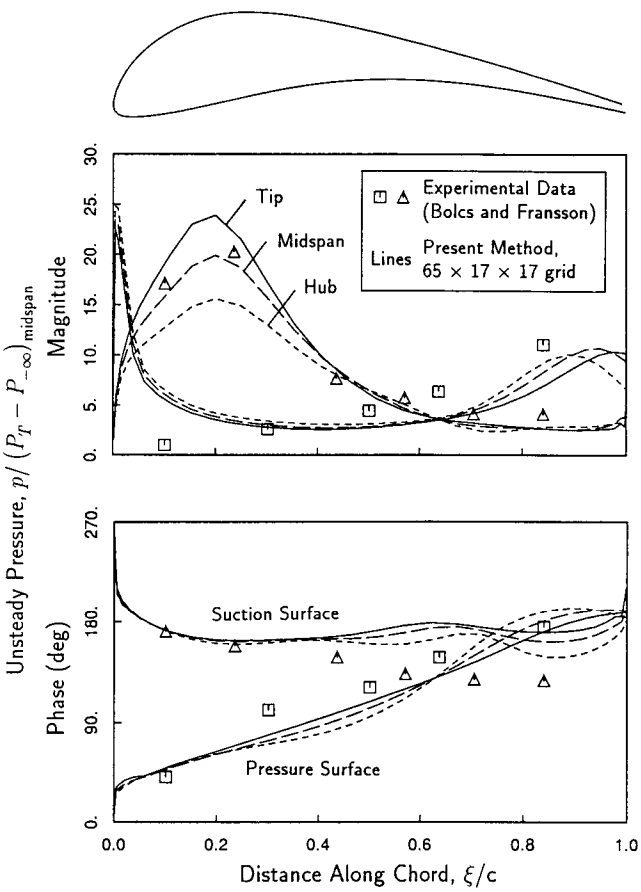

Figure 10: Unsteady pressure distribution on surface of airfoils of Fourth Standard Configuration turbine cascade undergoing plunging motion (Case 2). $\overline{\omega} = 0.13$, $\sigma = 90°$.

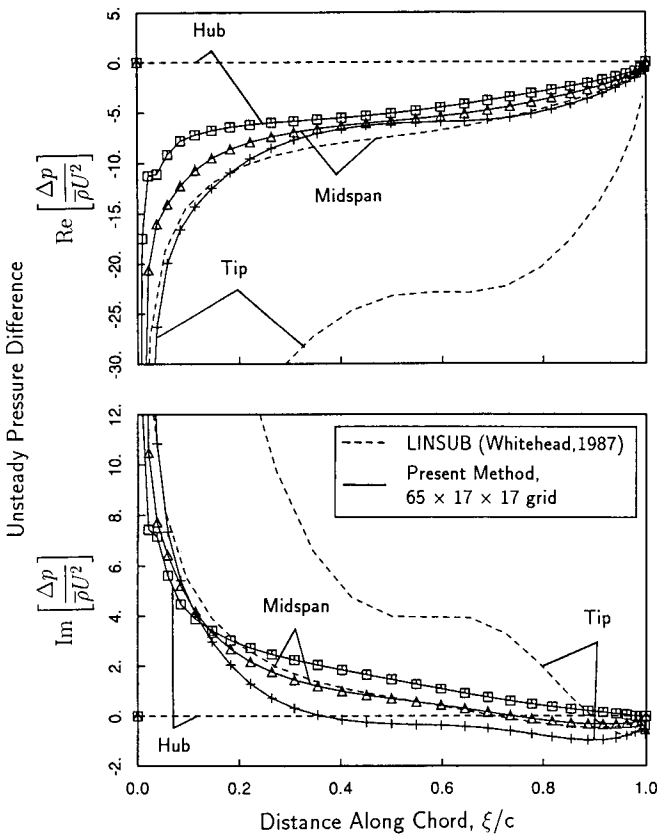

Figure 11: Unsteady pressure distribution on surface of reference airfoil of helical fan blade with airfoils vibrating in torsion about blade midchord. Pitching distribution is linear from hub to tip. $N = 18$, $AR_a = 2.0$, $c_a = 1.0$, $r_T = 4.0$, $r_H = 2.0$, $M_a = 0.5$, $\overline{\omega} = 0.4$, $\sigma = 180°$.

and phase of the computed unsteady pressure distribution. The agreement between the present theory and the experimental results, while not exact, certainly shows the correct trends. Note that the three-dimensional effects for this case are fairly small. This should not be too surprising as the experiment was designed to produce essentially two-dimensional results.

Subsonic Helical Fan

In this section, we consider an idealized fan geometry. The airfoils are helical surfaces and the advance ratio is such that the airfoils have zero steady pressure loading. The case considered here is of an 18-bladed rotor with a hub-to-tip ratio of 0.5. The axial chord of the blade, c_a, is 1.0, and the tip radius, r_T is 4.0. The mean flow axial Mach number, M_a, is 0.5. The rotational speed of the fan is such that the relative inflow angle, $\beta_{-\infty}$ at the midspan is 45°. For the unsteady case considered here, the blades pitch about their midchords with a reduced frequency, $\overline{\omega}$, of 0.4 based on axial chord and axial velocity, and the distribution of pitching amplitude is linear from hub to tip. Shown in Fig. 11 is the computed unsteady pressure difference across the airfoil surface. Also shown for comparison is the unsteady pressure difference predicted using Whitehead's LINSUB code (Whitehead, 1987) in a stripwise fashion. Note the generally poor agreement between the three-dimensional results and strip theory. Strip theory predicts that the response will be much larger at the tip than at the midspan or hub for two reasons. First, the dynamic pressure, which is proportional to the square of the relative velocity, is considerably larger at the tip. Second, the vibratory motion of the blade is largest at the tip. The unsteady pressure distributions found using the three-dimensional linearized Euler solver do not exhibit the strong spanwise variation in unsteady pressure predicted by strip theory. In fact, the imaginary part of the solution – the part which contributes to the aerodynamic damping – shows the opposite trend. These results have important implications on the prediction of flutter and forced response. For highly three-dimensional cascades, strip theory can be a poor predictor of aerodynamic damping.

CONCLUDING REMARKS

In this paper, we have presented a new three-dimensional linearized Euler solver that is capable of accurately and efficiently predicting unsteady small disturbance flows in turbomachinery blade rows. By using the pseudo-time time marching approach, well developed finite-volume schemes can be adapted to solve the linearized Euler equations in a fraction of the time required to compute the unsteady flow field using conventional time-accurate time marching algorithms. An important feature of the present analysis is the use of a deforming computational grid. The deformable grid eliminates the need to include large extrapolation terms in the moving blade boundary conditions and improves the accuracy of the method, especially for thin airfoils typical of those found in modern compressors and fans. For engineering applications, good results can be obtained using fairly coarse grids. Furthermore, for low to moderate reduced frequencies, the accuracy of the unsteady solution is on a par with the accuracy of the steady flow solution.

Computational results were compared to experimental results and other unsteady aerodynamic analyses. Preliminary results of the present analysis indicate that three-dimensional effects are significant for both linear and annular cascades. For example, it was found that strip theory can be a poor predictor of aerodynamic damping. Furthermore, three-dimensional effects change the character of the component of the unsteady pressure distribution which is out-of-phase with the upwash.

ACKNOWLEDGMENTS

This work was supported by a research contract from General Electric Aircraft Engines with Dr. Andrew Chuang serving as technical monitor. The authors wish to acknowledge helpful discussions with Dr. Graham Holmes of the General Electric Corporate Research and Development Center.

REFERENCES

Adamczyk, J. J., and Goldstein, M. E., 1978, "Unsteady Flow in a Supersonic Cascade with Subsonic Leading Edge Locus," *AIAA Journal*, Vol. 16, pp. 1248–1254.

Batina, J. T., 1990, "Three-Dimensional Flux-Split Euler Schemes Involving Unstructured Dynamic Meshes," AIAA Paper 90–1649.

Bölcs, A., and Fransson, T. H., 1986, Aeroelasticity in Turbomachines Comparison of Theoretical and Experimental Cascade Results, Air Force Office of Scientific Research, AFOSR–TR–87–0605.

Chi, R. M., 1991, "An Unsteady Lifting Surface Theory for Ducted Fan Blades," Presented at the International Gas Turbine

and Aeroengine Congress and Exposition, Orlando, FL. ASME Paper 91-GT-131.

Fourmaux, A., and Le Meur, A., 1987,"Computation of Unsteady Phenomena in Transonic Turbines and Compressors," Presented at the Fourth Symposium on Unsteady Aerodynamics and Aeroelasticity of Turbomachines and Propellers, Aachen University of Technology, Aachen, West Germany.

Fransson, T. H., 1991, Private communication.

Giles, M. B., 1988, "Calculation of Unsteady Wake/Rotor Interaction," *AIAA Journal of Propulsion*, Vol. 4, No. 4, pp. 356-362.

Giles, M. B., 1990, "Nonreflecting Boundary Conditions for Euler Equation Calculations," *AIAA Journal*, Vol. 28, pp. 2050-2058.

Gostelow, J. P., 1984, *Cascade Aerodynamics*, Pergamon Press, New York, Chapter 5.

Hall, K. C., and Crawley, E. F., 1989, "Calculation of Unsteady Flows in Turbomachinery Using the Linearized Euler Equations," *AIAA Journal*, Vol. 27, No. 6, pp. 777-787.

Hall, K. C. and Clark, W. S., 1991a, "Prediction of Unsteady Aerodynamic Loads in Cascades Using the Linearized Euler Equations on Deforming Grids," Presented at the AIAA/SAE/ASME/ASEE 27th Joint Propulsion Conference. AIAA Paper 91-3378.

Hall, K. C. and Clark, W. S., 1991b, "Calculation of Unsteady Linearized Euler Flows in Cascades Using Harmonically Deforming Grids," Presented at the Sixth Symposium on Unsteady Aerodynamics and Aeroelasticity of Turbomachines and Propellers, Notre Dame, IN.

Hall, K. C. and Verdon, J. M., 1991, "Gust Response Analysis for Cascades Operating in Non-Uniform Mean Flows," *AIAA Journal*, Vol. 29, No. 9, pp. 1463-1471.

Hall, K. C., 1992, "A Deforming Grid Variational Principle and Finite Element Method for Computing Unsteady Small Disturbance Flows in Cascades," Presented at the AIAA 30th Aerospace Sciences Meeting, Reno, NV. AIAA Paper 92-0665.

Holmes, D. G. and Chuang, H. A., 1991, "2D Linearized Harmonic Euler Flow Analysis for Flutter and Forced Response," Presented at the Sixth Symposium on Unsteady Aerodynamics and Aeroelasticity of Turbomachines and Propellers, Notre Dame, IN.

Huff, D. L., 1987, "Numerical Simulations of Unsteady, Viscous, Transonic Flow Over Isolated and Cascaded Airfoils Using a Deforming Grid." AIAA Paper 87-1316.

Huff, D. L. and Reddy, T.S.R., 1989, "Numerical Analysis of Supersonic Flow Through Oscillating Cascade Sections by Using a Deforming Grid." AIAA Paper 89-2805.

Namba, M., 1977, "Three-Dimensional Analysis of Blade Force and Sound Generation for an Annular Cascade in Distorted Flows," *Journal of Sound and Vibration*, Vol. 50, No. 4, pp. 479-508.

Namba, M., 1987, "Three-Dimensional Flows," Chapter 4 in AGARD Manual on Aeroelasticity in Axial-Flow Turbomachines, Unsteady Turbomachinery Aerodynamics, Vol. 1, M. F. Platzer and F. O. Carta (eds.), AGARD-AG-298.

Namba, M., and Toshimitsu, K., 1987, "Improved Double Linearization Method for Prediction of Mean Loading Effects on Subsonic and Supersonic Cascade Flutter," Presented at the Fourth Symposium on Unsteady Aerodynamics and Aeroelasticity of Turbomachines and Propellers, Aachen University of Technology, Aachen, West Germany.

Ni, R. H., and Sisto, F., 1976, "Numerical Computation of Nonstationary Aerodynamics of Flat Plate Cascades in Compressible Flow," *Transactions of the ASME: Journal of Engineering for Power* , Vol. 98, pp. 165-170.

Ni, R. H. and Bogoian, J. C., 1989, "Prediction of Three-Dimensional Multi-Stage Turbine Flow Field Using a Multiple-Grid Euler Solver," AIAA Paper 89-0203.

Rai, M. M., 1989a, "Three-Dimensional Navier-Stokes Simulations of Turbine Rotor-Stator Interaction; Part I - Methodology," *AIAA Journal of Propulsion and Power*, Vol. 5, No. 3, pp. 307-311.

Rai, M. M., 1989b, "Three-Dimensional Navier-Stokes Simulations of Turbine Rotor-Stator Interaction; Part II - Results," *AIAA Journal of Propulsion and Power*, Vol. 5, No. 3, pp. 312-319.

Saxer, A. P. and Giles, M. B., 1990, "Inlet Radial Temperature Redistribution in a Transonic Turbine Stage," AIAA Paper 90-1543.

Smith, S. N., 1972, "Discrete Frequency Sound Generation in Axial Flow Turbomachines," Aeronautical Research Council, London, Reports and Memoranda 3709.

Thompson, J. F., Thames, F. C., and Mastin, C. W., 1974, "Automatic Numerical Generation of Body-Fitted Curvilinear Coordinate System for Field Containing Any Number of Arbitrary Two-Dimensional Bodies," *Journal of Computational Physics*, Vol. 15, pp. 299-319.

Verdon, J. M., Adamczyk, J. J., and Caspar, J. R., 1975, "Subsonic Flow Past an Oscillating Cascade with Steady Blade Loading - Basic Formulation," Unsteady Aerodynamics, R. B. Kinney (ed.), University of Arizona, Tucson, AZ, pp. 827-851.

Verdon, J. M., and Caspar, J. R., 1984, "A Linearized Unsteady Aerodynamic Analysis for Transonic Cascades," *Journal of Fluid Mechanics*, Vol. 149, pp. 403-429.

Verdon, J. M., and McCune, J. E., 1975, "Unsteady Supersonic Cascades in Subsonic Axial Flow," *AIAA Journal*, Vol. 13, No. 2, pp. 193-201.

Whitehead, D. S., 1960, "Force and Moment Coefficients for Vibrating Aerofoils in Cascade," Aeronautical Research Council, London, Reports and Memoranda 3254.

Whitehead, D. S., 1962, "Bending Flutter of Unstalled Cascade Blades at Finite Deflection," Aeronautical Research Council, London, Reports and Memoranda 3386.

Whitehead, D. S., and Grant, R. J., 1981, "Force and Moment Coefficients of High Deflection Cascades," Proceedings of the 2nd International Symposium on Aeroelasticity in Turbomachines, P. Suter (ed.), Juris-Verlag Zurich, pp. 85-127.

Whitehead, D. S., 1987, "Classical Two-Dimensional Methods," Chapter 2 in AGARD Manual on Aeroelasticity in Axial-Flow Turbomachines, Unsteady Turbomachinery Aerodynamics, Vol. 1, M. F. Platzer and F. O. Carta (eds.), AGARD-AG-298.

Whitfield, D. L., Swafford, T. W., and Mulac, R. A., 1987, "Three-Dimensional Unsteady Euler Solutions for Propfans and Counter-Rotating Propfans in Transonic Flow," Presented at the AIAA 19th Fluid Dynamics, Plasma Dynamics, and Lasers Conference, Honolulu, HI. AIAA Paper 87-1197.